Nanoscale

Accepted Manuscript

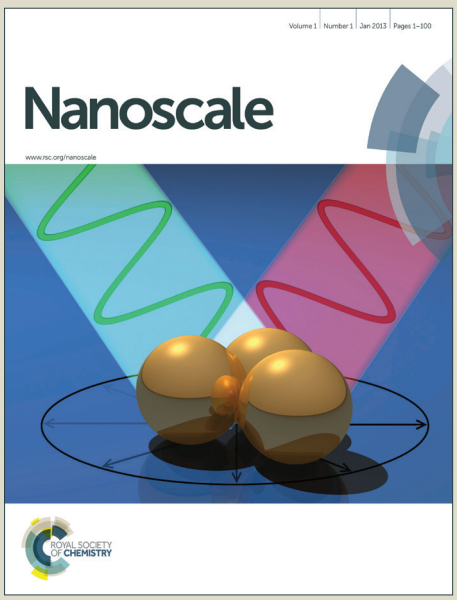

ROYAL SOCIETY OF CHEMISTRY

www.rsc.org/nanoscale

Journal Name

ARTICLE

Multilayer Silicene: The Bottom-Up Approach for a Weakly Relaxed Si(111) with Dirac Surface States

Received 00th July 2015,
Accepted 00th January 20xx

DOI: 10.1039/x0xx00000x

www.rsc.org/

Huixia Fu, Lan Chen, Jian Chen, JinglanQiu, Zijing Ding, Jin Zhang, Kehui Wu, Hui Li*, Sheng Meng*

Combining first principles investigations and scanning tunneling microscopy, we identify that the presumable van der Waals packed multilayer silicene sheets spontaneously transform into diamond-structure bulk Si film due to strong interlayer couplings. In contrast to drastic surface reconstruction on conventional Si(111), multilayer silicene prepared by bottom-up epitaxy on Ag(111) exhibits nearly ideal flat surface with only weak buckling. Without invoking Ag surfactants, √3×√3 honeycomb patterns emerge thanks to dynamic fluctuation of mirror-symmetric rhombic phases, similar to monolayer silicene [Chen et al., Phys. Rev. Lett. 110, 085504 (2013)]. The weak relaxation enables novel surface states with a Dirac linear dispersion.

1. Introduction

Silicene, the silicon layer in a honeycomb lattice analogous to graphene, is emerging as a two-dimensional quantum material which hosts relativistic Dirac fermions and stronger spin-orbital interactions than its carbon counterpart [1-4]. The past three years have witnessed a burst in silicene research: Single-layer silicene (SLS) has been experimentally grown on Ag(111) and other substrates [5-17]. Multilayer silicene (MLS) also draws intensive attentions, e.g., in chiral superconducting behavior [18], valley-polarized quantum Hall effect [19], and dramatically tunable electronic structure by varying stacking modes [20,21]. By now, MLS films have been grown by several groups on Ag(111) using molecular beam epitaxy (MBE) [22-28].

Despite intensive efforts based on scanning tunneling microscopy (STM) and spectroscopy (STS), angle-resolved photoemission spectroscopy (ARPES), and first principles modeling, the atomic structure and electronic features of epitaxial silicene remain heavily debated. Various metastable relaxations were observed for SLS on Ag(111) [5-14]. Among them the √3×√3-*R*30° (abbreviated as √3) structure is believed the closest to free-standing silicene, since it exhibits reversible dynamical phase transitions at low temperatures and weak bonding to substrate [14]. Quasiparticle interference (QPI) pattern analysis from STS mapping reveals linear band dispersions in √3 structure, also close to isolated silicene [14]. The 3×3 superstructure (respecting to the lattice of Si) is stable but the absence of Landau levels in magnetic field [29] casts doubts on the presence of Dirac fermions. First principles calculations also imply that the Dirac state in 3×3 phase [30] and other monolayer phases [31,32] is destroyed by strong Si-Ag interaction, and linear band dispersion observed in ARPES [10] might actually come from silver substrate [30,33,34].

Recent experiments show multilayer silicene on Ag(111) can grow up to ~50 layers (L) with a unique √3 surface relaxation [24-28,35,36]. Padova*et al.* propose MLS takes van der Waals packing between Si layers according to height measurements of Si layers and vibration spectra [26], while Mannix*et al.* thought MLS adopts diamond packing as bulk silicon [35]. Shirai*et al.*[36] argue that √3 relaxation in MLS might come from the Si(111)-√3×√3-Ag surface [37], but they freely admit this model cannot explain ultralow phase transition temperature and ARPES band structures, thus clean √3 surface might also exist. In addition, although there are significant differences in MLS and SLS atomic structures, similar Dirac fermion states are observed for both of them [24,28], with the position and slope of Dirac bands independent of film thickness. Recently, Zhuang *et al.* also observed the Dirac point of epitaxial √3×√3 silicene at 0.33 eV below the Fermi level using ARPES [38]. Therefore, it is of crucial importance to clarify in theory the atomic structure of multilayer silicene and the relation to its monolayer counterpart, as well as the origin of observed Dirac bands.

Here we present a systematic first-principles study on the epitaxial and free-standing multilayer silicene. Surprisingly, the presumable van der Waals stacked silicene layers spontaneously transform into diamond ABC stacking as in bulk Si(111). Calculations reveal that *clean* surface of epitaxial MLS adopt a universal √3 relaxation in consistence to STM observations, while the same √3 relaxation shows up for free-standing MLS with a thickness θ ≥ 3 L. The weak √3 relaxation only involves atom buckling without bond breaking/reforming and is radically different from drastic

Beijing National Laboratory for Condensed Matter Physics and Institute of Physics, Chinese Academy of Sciences, Beijing 100190, China
Address correspondence to huili8@iphy.ac.cn;smeng@iphy.ac.cn
† Electronic Supplementary Information (ESI) available: [Definition of cohesive and binding energies; Atomic structures of 5-layer MLS in two mirror-symmetric √3 phases; Band structures of Ag(111) surface, free-standing and epitaxial MLS films; Atomic structures, band structures, and simulated STM images for Si(111)-√3×√3-Ag layer; STM observations in surface layer peeling-off experiment.Definition of cohesive and binding energies; Atomic structures of 5-layer MLS in two mirror-symmetric √3 phases; Band structures of Ag(111) surface, free-standing and epitaxial MLS films; Atomic structures, band structures, and simulated STM images for Si(111)-√3×√3-Ag layer; STM observations in surface layer peeling-off experiment.]. See DOI: 10.1039/x0xx00000x

reconstruction on conventional Si(111). According to our calculations, clean MLS films with weak surface relaxation exhibit robust surface states which cross at Fermi level with nearly linear dispersion, explaining the Dirac bands observed in ARPES and STS [28,39].

2. Methods

First-principles calculations were performed using conventional Perdew-Burke-Ernzerhof (PBE) functional [40] in Vienna Ab initio Simulation Package (VASP) [41], combined with projector-augmented wave (PAW) pseudopotentials, and the plane-wave basis set with energy cutoff at 250 eV. The 3×3 supercells of silicene thin films (1-5 silicon layers) on a five-layer 4×4 Ag(111) slab (in experimental lattice constant of 11.56 Å) were chosen. All the structures were fully relaxed with the bottom two layers of Ag atoms fixed. A vacuum region of ≥15 Å is applied, and the Brillouin zone is sampled by 5×5×1 Monkhorst-Pack *k*-mesh. The STM images were collected in an ultra-high-vacuum chamber at 77 K, with STS mapping extracted from lock-in signals by applying a modulation of 20 mV at 777 Hz to the tip bias. Silicon was evaporated from heated Si wafer with a deposition flux of ~0.3 layers per minute.

3. Results and discussions

3.1Structure of multilayer silicene on Ag(111).

To mimic MLS growth mode in MBE experiment, atomic structures are relaxed by adding free-standing single-layer silicon onto Si/Ag(111) in a layer-by-layer fashion. The initial structure is set to either AA or AB stacking at layer heights >4 Å. Relaxed structural parameters are listed in Table I.

As reported previously a rhombic √3 superstructure for SLS on Ag(111) is found, where 1/6 Si atoms are highly buckled with a height ~1.1 Å while other Si atoms are nearly flat (Fig. 1(a, d)). When a second Si layer is added to SLS/Ag(111), the initially van der Waals stacked silicene bilayer (characterized by a large interlayer distance >4 Å) spontaneously form covalent bonds between the two layers. This can be understood as the buckled SLS is quite active whose π bonds made of Si p_z orbitals easily break up to form sp^3 bonds. Unlike isolated bilayer silicene (BLS) with various stacking modes [20], only AB stacking is found for BLS/Ag(111). The top layer of BLS also exhibits a √3 structure similar to SLS, while the bottom layer adopts bulk Si(111) structure (Fig. 1(b, e)).

By adding additional Si adlayers above the bilayer, diamond bulk structure spontaneously forms. Structure optimization produces only the ABC layer stacking irrespective the initial packing position. Interestingly, the surface of all MLS films displays √3 relaxation, while Si layers beneath the top layer adopt ordinary diamond lattice, see Fig. 1(c, f) for 5-layer MLS/Ag. Therefore, we conclude √3 relaxation is a universal feature for silicon monolayer to multilayer on Ag(111).

Calculated atomic structures are in agreement with experiment. Fig. 2(a-c) displays STM images for coexisting 1~3 layers of silicon films on Ag(111). The √3 honeycomb superstructure and ABC stacking are clearly demonstrated by super-positioning atomic structural models onto STM images. Atomic heights measured by STM for the top Si layer (3.15~3.20 Å, Fig. 2(d)) also agree with the calculated values (3.18-3.30 Å, Table I).

TABLE I. Structural parameters for the 1-5 Si layers (L) with and without Ag substrate. $\Delta Z_{1\text{-}5}$ (Å), the buckling distance of each Si layer; *h* (Å), the thickness of the top Si layer; E_c(eV/Si), the cohesive energy per Si atom; E_{b1} (eV/Si) and E_{b2} (eV/Si), binding energies for interlayer Si-Si bonds and Si-Ag bonds.

	ΔZ_1	ΔZ_2	ΔZ_3	ΔZ_4	ΔZ_5	*h*	E_c	E_{b1}	E_{b2}
1L/Ag	1.03	-	-	-	-	3.30	4.34	-	0.44
2L/Ag	0.81	0.98	-	-	-	3.26	4.32	0.41	0.58
3L/Ag	0.82	0.79	1.08	-	-	3.26	4.38	0.58	0.63
4L/Ag	0.83	0.79	0.80	1.10	-	3.24	4.41	0.63	0.66
5L/Ag	0.83	0.79	0.79	0.80	1.10	3.18	4.44	0.63	0.66
1L	0.47	-	-	-	-	-	3.90	-	-
2L	0.67	0.67	-	-	-	3.23	4.03	0.26	-
3L	1.20	0.80	1.21	-	-	3.71	4.16	0.52	-
4L	1.23	0.80	0.80	1.22	-	3.25	4.25	0.60	-
5L	1.22	0.80	0.79	0.80	1.23	3.17	4.31	0.63	-
Bulk Si	0.79	0.79	0.79	-	-	3.16	4.61	-	-

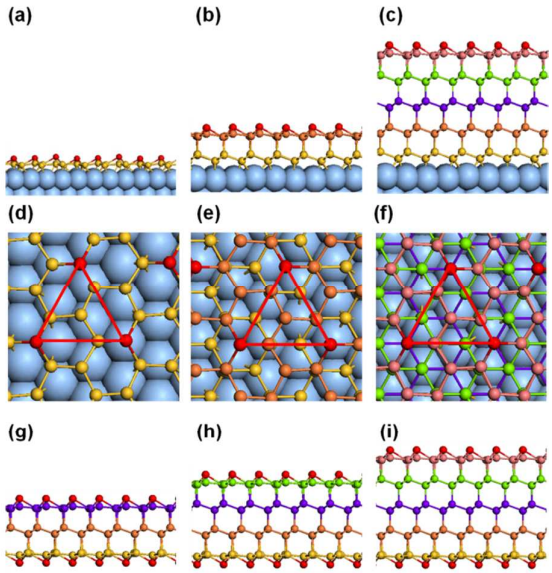

Figure 1. (a-c) Side and (d-f) top views of monolayer, bilayer, and 5-layer Si(111) films on Ag(111). (g-i) Side views of 3-, 4-, 5-layer free-standing Si(111) thin films. Small and large spheres denote Si and Ag atoms, respectively. Different colours denote Si in different atomic layers, and the outmost buckling Si atoms are red coloured. Red triangles in (g-i) denote the √3 surface relaxation.

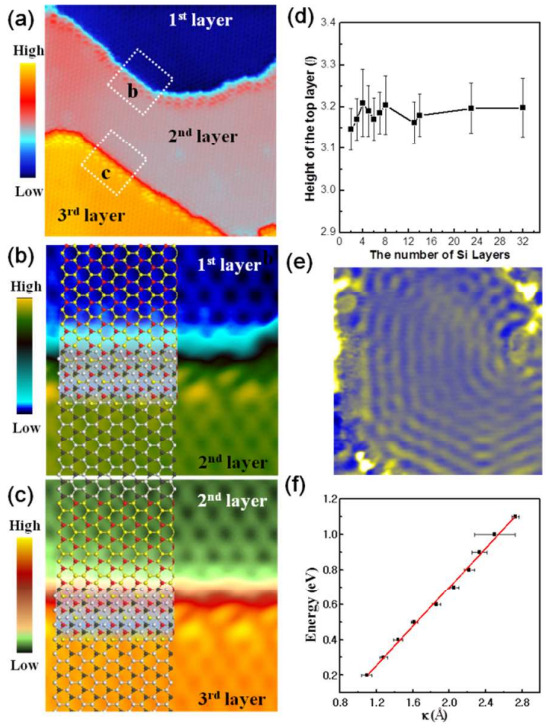

Figure 2. (a) Scanning tunneling microscopy (STM) image (V_{tip} = 1.2 V, 25×25 nm^2) of Si films on Ag(111). (b) and (c) High resolution STM images of the area labeled by white squares in (a). The atomic structure of the √3×√3 silicene is superimposed, indicating that the stacking sequence of the neighbor Si layers is cubic ABC stacking. (d) The measured height of topmost layer on multilayer Si on Ag(111). (e)dI/dV map (V_{tip} = −0.4 V, 20×20 nm^2) on the surface of 8 layers Si film with obvious standing waves of surface states. (f) The linear energy-momentum dispersion by measuring the wavelength of standing waves in dI/dV maps under different bias.

3.2 Structure of free-standing multilayer silicene

To understand the effect of Ag substrate in MLS formation, we study free-standing MLS films without Ag(111) substrate. Both Si monolayer and bilayer turn back into the 1×1 low-buckled structure when Ag(111) is peeled off, indicating the substrate is the key for maintaining √3 relaxation for SLS and BLS. The buckling height of each Si layer in BLS (0.67 Å) is slightly larger than in monolayer (0.47 Å), but smaller than that for bulk Si (0.79 Å), suggesting more unsaturated Si atoms make silicon layers flatter. For free-standing MLS thicker than 3 layers, the √3 superstructure starts to form automatically on both surfaces. They also show an ABC stacking mode (Fig. 1(g-i)). The √3 superstructure exists for both epitaxial and free-standing MLS with a thickness θ≥3 layers, indicating this is a universal surface feature for Si thin films, irrelevant to substrate effects.

For silicene on Ag(111), the Si-Ag interaction is close to Si-Si covalent bond, considering the Si-Ag bond length (~2.6 Å) is close to Si-Si bonds (~2.3 Å) and the electronegativity of Ag and Si atoms is also similar. This is further supported by similar binding energies (0.40~0.65 eV/Si) for both interlayer Si-Si (E_{b1} in Table I) and Si-Ag bonds (E_{b2}). As a result, silicene on Ag behaves like a thicker free-standing MLS, as the Ag substrate serves as the role of additional Si layers. This explains √3 surface relaxation, universal for thick Si films, emerges even for SLS/Ag(111). We note √3 relaxation was also observed on Ir(111) and ZrB_2(0001) [7,8].

3.3 Stability of multilayer silicene.

The cohesive energies E_c (see details in Supporting Information) for MLS sheets with and without Ag(111) substrate are plotted in Fig. 3(a). The E_c of isolated MLS increases significantly from 1 to 5 layers, towards a limiting value of 4.61 eV/Si, the E_c for bulk. MLS films on Ag(111) have a larger cohesive energy, increasing only slightly with film thickness, due to stabilization by the substrate. The epitaxial BLS has a smallest E_c, implying it is not particularly stable with respect to thinner or thicker MLS [35].

Similar to the SLS case [14], two mirror-symmetric rhombic √3×√3 phases are also observed for the topmost Si layer of MLS. The energy barrier for switching between the two energy-degenerate phases is low (5-30 meV/Si), leading to fluctuating honeycomb structure observed in Fig. 2. The energy barrier between such two configurations increases as the MLS thickness θ increases and saturates at θ= 4-5 layers, see Fig. 3(b). The transition is more difficult for thicker Si films, making observation of rhombic patterns at elevated temperature possible.

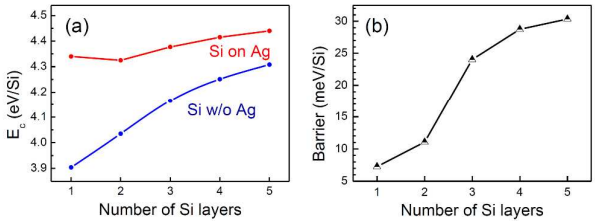

Figure 3. (a) Cohesive energy versus the number of Si layers with (red) and without (blue) substrate. (b) Energy barrier for structural transition between the two mirror-symmetric √3 configurations of MLS/Ag(111).

3.4 Electronic structures

Band structures of isolated and epitaxial MLS films are calculated with the high-symmetry paths sampled in the Brillouin zones referred to the3×3 boundary for Si (4×4 boundary for Ag). The bands are projected onto each atomic layer of Si and Ag to understand their respective contributions. Free-standing SLS has a Dirac cone band structure around the Fermi level (Fig. 4(a)), whose lower half and upper half corresponds to the π and π* bands made of Si p_z orbitals. On Ag(111), the Dirac cone of epitaxial SLS is absent due to interface Si-Ag interaction [30]. Projected band plots in Fig. 4(f) show that the vertexes of lower half (π orbital) and upper half (π* orbital) shift to −0.8 and 0.8 eV respectively, leading to a gap of ~1.6 eV. Meanwhile, the linear dispersion bands become parabolic at vertexes. Interestingly, a cone-like structure with linearly dispersion is found at −0.35 eV for the bands projected onto Ag (Fig. S4(k)). Such bands are a result of band folding from Ag substrate (Fig. S2)

induced by the extended periodicity of adsorbed silicene[28], and remain unchanged for thicker silicon films (Fig. S4(l-o)). Projected band structures onto each Ag layer (Fig. S5(f-j)) also suggest the "Dirac cone" at −0.4 eV indeed originates from the states of bulk silver.

Free-standing 2~5-layer Si sheets exhibit metallic band structures. This is in contrast to an energy gap of ~0.75 eV found for bulk Si calculated on the same level of theory (Fig. S3). BLS has maintained the linear dispersion bands, while new parabolic bands also show up with vertexes at ±0.5 eV (Fig. 4(b)). The vertexes move toward the Fermi level with increasing thickness, and they touch to form a cone-like band structure for thickness θ ≥4 layers (Fig. S4(d, e)). Analysis on the local density of states demonstrates that the new bands come from the dangling bonds of flat-lying Si atoms in the outmost layer, namely the surface states of MLS films (Fig. 4(j)). As shown in Fig. 4(g-j), these surface states survive upon adsorption on Ag(111), since the top surface is not affected by interface bonding. This is further evidenced by bands decomposition onto each atomic layer displayed in Fig. S5.

By fitting to the linear surface bands in Fig. 4(j), a Fermi velocity v_F of 0.36×10^6 m/s is resulted, in excellent coincidence to the value measured in ARPES, 0.3×10^6 m/s [28]. If a parabola is used to fit the bottom of the cone, an effective electron mass of 0.14 m_e (m_e is free electron mass) is obtained for 5-layer MLS, an effective electron mass of 0.14 me (me is free electron mass) is obtained for 5-layer MLS. Similar value for 2-layer MLS on Ag(111) (0.15m_e) is identical to that measured by STS [39], but different from that for Ag surface bands (0.40 m_e). Our STS maps on an 8-layer MLS clearly displays standing waves of surface state, which gives a linear band dispersion but with a large v_F 0.9×10^6 m/s (Fig. 2(e,f)). The Bader charge analysis also has been applied to study the charge transfer of MLS/Ag(111) system. As shown in TABLE S2, the electron of 0.46-0.83 e is found to transfer from Si to Ag substrate. From Fig. 4(g-j), the linear band dispersion from topmost Si layer is found at the position of slightly above Fermi level. The lower Dirac point below Fermi level reported in experiment [28,38,39] might be a result of surface charging effect.

3.5 MLS versus Si-Ag alloy surface

It is well known the Ag atoms on Si(111) surface can also induce a √3×√3 surface reconstruction, leading to Si(111)-√3×√3-Ag surface, which has been well studied in past two decades. Pioneer experiments at high annealing temperature (400 °C) demonstrated that the STM images of pure √3 MLS and Si(111)-√3×√3-Ag surface may be similar [36]. To compare the difference between these two surfaces, we calculated the structure of Si(111)-√3×√3-Ag surfaceas shown in Fig. S6-S9. Despite the similarity in structures and STM images (Fig. S6-S7), strong parabolic surface state of Si(111)-√3×√3-Ag surface was also obtained, as shown in Fig. S8. However, significant differences of Ag-Si alloy surface were also observed, such as smaller effective electron mass (0.09 m_e) than it of MLS. The Si(111)-√3×√3-Ag surface was rougher (mean square displacement, MSD ~ 0.05 Å^2) than MLS on Ag(111) (MSD ~0.006 Å^2, see Table S1 and Fig. S9). Furthermore, structure phase transition was reported to take place above 120 K for Si(111)-√3×√3-Ag surface [42], while it happens at ~40 K in MLS in our experiment. In addition, an extra peel-off experiment was performed to further confirm MLS surface. As shown in Fig. S10, the top layer of synthesized MLS was peeled off by a bias pulse, and the underneath Si surface, which should be Ag-free, still exhibits a √3×√3 reconstruction, as displayed in Fig. S10. In addition, it is emphasized that the choice of Ag(111) substrate and growing temperature may play key factors to grow pure MLS surface. High quality Ag(111) single crystal and low annealing temperature (< 500 K) can significantly reduce the opportunity for Ag atoms diffusing to silicon surface.

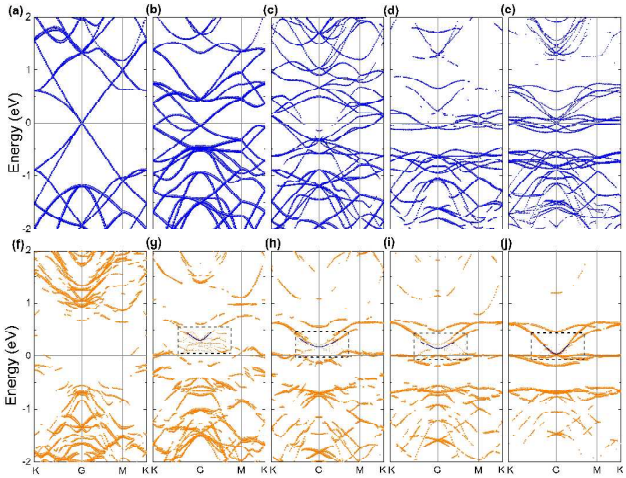

Figure 4. Projected band structures on the topmost silicon atomic layers for (a-e) isolated 1-5 layer Si(111) films and (f-j)corresponding epitaxial Si (111) films bonded on Ag substrate. The size of dots corresponds to the contribution weight. The squares denote the range of Dirac cone, and the vertexes of surface states are emphasized by blue lines in the squares.

4. Conclusions

It is well known that conventional bulk Si(111) exhibits drastic surface reconstruction including Si(111)-2×1, Si(111)-5×5, and the complex Si(111)-7×7 as described in the dimer-adatom-stacking fault (DAS) model. The Si(111)-2×1 surface is a reconstruction of cleaved Si(111), and Si(111)-5×5 and Si(111)-7x7 phases require high temperature annealing treatment at above 800°C and involves significant bond breaking/reforming to saturate local dangling bonds [43-48]. Based on the first principles calculations, all these three reconstruction Si(111) surfaces show better stability than non-reconstructed Si(111) surface, and the √3 relaxation also increases the stability of Si(111), as listed in Table II. Thus, ideal Si(111)-1×1 surface is absent from traditional treatments based on single crystal cleavage and/or high temperature annealing. Here the low temperature (<300°C; Si film desorbs at higher temperature) epitaxial growth of MLS thin film represents a new bottom-up approach to synthesize nearly ideal Si(111) surface. The weak √3 buckling preserves the original hexagonal bond topology and leaves most Si atoms (5 out of 6) in ideally flat-lying positions to form delocalized π bonds, therefore the Dirac band structure originated from low-bulked Si survives. No surfactant Ag is needed to achieve √3 surface relaxation and linear dispersion bands [37]. This provides an idea model system

to study weakly- or non-reconstructed Si surface with novel electronic characteristics.

TABLE II. Cohesive energies of 5-layer Si(111) films with common reconstructed surfaces.

	7×7	5×5	2×1	√3×√3 (MLS)	1×1
E_c(eV/Si)	4.356	4.340	4.325	4.308	4.287

Acknowledgements

This work was supported by the "973" Project of China (2012CB921403, 2013CBA01600, 2012CB921703), NSFC (Grant Nos. 11334011, 11222431, 11322431), "Strategic Priority Research Program" of the Chinese Academy of Sciences, and Hundred Talent Program of IOP, CAS.

References

1. G. G. Guzman-Verri and L. C. Lew Yan Voon,*Phys. Rev. B,* 2007, **76**, 075131.
2. C. C. Liu, W. Feng, and Y. G. Yao, *Phys. Rev. Lett.,* 2011, **107**, 076802.
3. C. C. Liu, H. Jiang, and Y. G. Yao, *Phys. Rev. B,* 2011, **84**, 195430.
4. M. Ezawa, *Phys. Rev. Lett.*, 2012, **109**, 055502.
5. L. Chen, C. C. Liu, B. Feng, X. He, P. Cheng, Z. Ding, S. Meng, Y. G. Yao, and K. H. Wu, *Phys. Rev. Lett.,*2012, **109**, 056804.
6. B. Feng, Z. J. Ding, S. Meng, Y. G. Yao, X. Y. He, P. Cheng, L. Chen, and K. H. Wu, *NanoLett*., 2012, **12**, 3507–3511.
7. A. Fleurence, R. Friedlein, T. Ozaki, H. Kawai, Y. Wang, and Y. Yamada-Takamura, *Phys. Rev. Lett.,* 2012, **108**, 245501.
8. L. Meng, Y. Wang, L. Zhang, S. Du, R. Wu, L. Li, Yi Zhang, G. Li, H. Zhou, W. A. Hofer, and H. J. Gao, *NanoLett.,* 2013, **13**, 685–690.
9. D. Chiappe, E. Scalise, E. Cinquanta, C. Grazianetti, B. Broek , M. Fanciulli, M. Houssa, and A. Molle, *Adv. Mater.,* 2014, **26**, 2096.
10. P. Vogt, P. De Padova, C. Quaresima, J. Avila, E. Frantzeskakis, M. C. Asensio, A. Resta, B. Ealet, and G. Le Lay, *Phys. Rev. Lett.,* 2012, **108**, 155501.
11. C. L. Lin, R. Arafune, K. Kawahara, N. Tsukahara, E. Minamitani, Y. Kim, N. Takagi, and M. Kawai, *Appl. Phys. Exp*., 2012, **5**, 045802.
12. H. Jamgotchian, Y. Colington, N. Hamzaouri, B. Ealet, J. Hoarau, B. Aufray, and J. P. Biberian, *J. Phys. Condens. Matter,* 2012, **24**, 172001.
13. D. Chiappe, C. Grazianetti, G. Tallarida, M. Fanciulli, and A. Molle, *Adv. Mater.,* 2012, **24**, 5088.
14. L. Chen, H. Li, B. Feng, Z. Ding, J. Qiu, P. Cheng, K. H. Wu, and S. Meng, *Phys. Rev. Lett.,* 2013, **110**, 085504.
15. L. Chen, C.-C. Liu, B. Feng, X. He, P. Cheng, Z. Ding, S. Meng, Y. Yao, and K. Wu, *Phys. Rev. Lett.*, 2013, **110**, 229702.
16. L. Chen, B. Feng, and K. Wu, *Appl. Phys. Lett.,* 2013, **102**, 081602.
17. B. Feng, H.Li, C.-C. Liu, T. Shao, P. Cheng, Y. Yao, S. Meng, L. Chen and K. Wu, *ACS Nano*, 2013, **7**, 9049.
18. F. L. Liu, C. C. Liu, K.H. Wu, F. Yang, and Y. G. Yao, *Phys. Rev. Lett.,* 2013, **111**, 066804.
19. H. Pan, Z. Li, C.-C. Liu, G. Zhu, Z. Qiao, and Y. Yao,*Phys. Rev. Lett.,* 2014, **112**, 106802.
20. H. Fu, J. Zhang, Z. Ding, H. Li, and S. Meng**,** *Appl. Phys. Lett.***,** 2014, **104***,* 131904.
21. J. Bai, H. Tanaka and X. C. Zeng, *Nano Res.,* 2010, **3**, 694.
22. P. D. Padova, O. Kubo, B. Olivieri, C. Quaresima, T. Nakayama, M. Aono, and G. L. Lay, *NanoLett.,*2012, **12**, 5500.
23. T. Morishita, M. J. S. Spencer, S. P. Russo, I. K. Snook, and M. Mikami, *Chem. Phys. Lett.,* 2011, **506**, 221.
24. P. D. Padova, J. Avila, A. Resta, I. R.-Colambo, C. Quaresima, C. Ottaviani, B. Olivieri, T. Bruhn, P. Vogt, M. C. Asensio, and G. L. Lay, *J. Phys.: Condens. Matter,* 2013, **25**, 382202.
25. P. Vogt, P. Capiod, M. Berthe, A. Resta, P. De Padova, T. Bruhn, G. Le Lay, and B. Grandidier, *Appl. Phys. Lett.,* 2014, **104**, 021602.
26. P. D. Padova, C. Ottaviani, C. Quaresima, B. Olivieri, P. Imperatori, E. Salomon, T. Angot, L. Quagliano,C. Romano, A. Vona, M. Muniz-Miranda, A. Generosi, B. Paci and G. L. Lay, *2D Materials,* 2014, **1**, 021003.
27. J. Chen, W. Li, B. Feng, P. Cheng, J. Qiu, L. Chen, and K. Wu,arXiv:1405.7534.
28. P. D. Padova, P. Vogt, A. Resta, J. Avila, I. R.-Colambo, C. Quaresima, C. Ottaviani, B. Olivieri, T. Bruhn, T. Hirahara, T. Shirai, S. Hasegawa, M. C. Asensio, and G. L. Lay,*Appl. Phys. Lett.,* 2013, **102**, 163106.
29. C. L. Lin, R. Arafune, K. Kawahara, M. Kanno, N. Tsukahara, E. Minamitani, Y. Kim, M. Kawai, and N. Takagi, *Phys. Rev. Lett.,* 2013, **110**, 076801.
30. D. Tsoutsou, E. Xenogiannopoulou,E. Golias,P. Tsipas andA. Dimoulas,*Appl. Phys. Lett.,*2013, **103**, 231604.
31. Y. Yuan, R. Quhe, J. Zheng, Y. Wang, Z. Ni, J. Shi, J. Lu, *Physica E*, 2013, **11**, 16.
32. R. Quhe,Y. Yuan,J. Zheng,Y. Wang,Z. Ni,J. Shi,D. Yu, , and J. Lu, *Scientific Reports,* 2014, **4**, 5476.
33. P. Gori,O. Pulci,F. Ronci,S. Colonna, andF. Bechstedt,*J. Appl. Phys.,*2013, **114**, 113710.
34. Z. X. Guo and A. Oshiyama, *Phys. Rev. B,* 2014, **89**, 155418.
35. A. J. Mannix, B. Kiraly, B. L. Fisher, M. C. Hersam, and N. P. Guisinger,*ACS Nano,* 2014, **8**, 7538.
36. T. Shirai, T. Shirasawa, T. Hirahara, N,Fukui, T. Takahashi, and S. Hasegawa,*Phys. Rev. B,* 2014, **89**, 241403.
37. N. Sato, S. Takeda, T. Nagao, and S. Hasegawa, *Phys. Rev. B,* 1999, **59**, 2035–2039.
38. J. Zhuang, X. Xu, Y. Du, K. Wu, L. Chen, W. Hao, J. Wang, W. K. Yeoh, X. Wang, S. X. Doul, *Phys. Rev. B,* 2015, **91**, 161409.
39. R. Arafune, C.-L. Lin, R. Nagao, M. Kawai, and N. Takagi,*Phys. Rev. Lett.,* 2013, **110**, 229701.
40. J. P. Perdew, K. Burke, and M. Ernzerhof, *Phys. Rev. Lett*., 1996, **77**, 3865.
41. G. Kresse and J. Furthmüller, *Phys. Rev. B*, 1996, **54**, 11169.
42. H. Tajiri, K. Sumitani, S. Nakatani, A. Nojima, T. Takahashi, K. Akimoto, H. Suiyama, X. Zhang, and H. Kawata, *Phys. Rev. B*, 2003, **68**, 035330.
43. R. E. Schlier and H. E. Farnsworth, *J. Chem. Phys.*, 1959, **30**, 917.
44. G. Binning, H. Rohrer, Ch. Gerber, and E. Weibel, *Phys. Rev. Lett*., 1983, **50**, 120.
45. A. Bennett, L. C. Feldman, Y. Kuk, E. G. McRae, and J. P. Rose, *Phys. Rev. B*, 1983, **28**, 3656.
46. E. G. McRae and C. W. Caldwell, *Phys. Rev. Lett.*, 1981, **46**, 1632.

47. E. G. McRae, *Phys. Rev. B*, 1983, **28**, 2305.
48. K. Takayanagi, Y. Tanishiro, M. Takahashi, and S.Takahashi, *J. Vac. Sci. Technol. A*, 1985, **3**, 1502; *Surf. Sci.*, 1985, **164**, 367.